Carbohydrate Polymers 102 (2014) 813–820

Contents lists available at ScienceDirect

Carbohydrate Polymers

journal homepage: www.elsevier.com/locate/carbpol

Synthesis, characterization, and *in vitro* studies of graphene oxide/chitosan–polyvinyl alcohol films

Andreea Madalina Pandele[a], Mariana Ionita[a,*], Livia Crica[a], Sorina Dinescu[b], Marieta Costache[b], Horia Iovu[a]

[a] University Politehnica of Bucharest, 132 Calea Grivitei, 010737 Bucharest, Romania
[b] University of Bucharest, Splaiul Independentei 91-95, 050095 Bucharest, Romania

ARTICLE INFO

Article history:
Received 16 July 2013
Received in revised form 14 October 2013
Accepted 29 October 2013
Available online 5 November 2013

Keywords:
Chitosan–polyvinyl alcohol
Graphene oxide
Nanocomposite
Mechanical strength
Cells culture

ABSTRACT

Nanocomposites based on chitosan–polyvinyl alcohol (CS–PVA) and graphene oxide (GO) were prepared by casting the stable aqueous mixture of the components. SEM, TEM and X-ray diffraction showed that graphene oxide is largely dispersed on molecular scale within CS–PVA matrix. FTIR investigation indicated the occurrence of some interaction between graphene oxide nanosheets and CS–PVA. The obtained composites are mechanically strong and exhibit improved thermal stability. By addition of 6 wt.% GO within CS–PVA blend, the elastic modulus increased over 200%. The cell viability and proliferation results showed that MC3T3-E1 mouse osteoblastic cells can adhere and developed on the CS–PVA/GO composite films. A significant proliferation potential was displayed by the cells in contact with CS–PVA/GO 6 wt.%. Graphene oxide reinforced CS–PVA with high mechanical and bioactive properties are potential candidates for tissue engineering.

© 2013 Elsevier Ltd. All rights reserved.

1. Introduction

In recent years, carbon nanotubes (CNTs) have been considered ideal reinforcing agent for polymer matrices due to their unique structure and remarkable properties (Li, Fan, & Watari, 2010). CNTs-polymer composites have attracted an increasing attention in biomedical field for application such as tissue engineering, drug delivery, diagnosis, *etc*., (Bianco, Kostarelos, & Prato, 2005; Xiaodong, Hua, Chang, & Lucian, 2010). Despite the advantageous properties, CNTs are not considered favorable as biomaterials because of the toxic nature of the impurities from the synthesis and the hydrophobic character leading to agglomeration of the particles and therefore poor dispersion in biological media (Depan, Shah, & Misra, 2011). New studies showed that it is preferable to use a metal-free material to enhance or gain new properties to polymeric biomaterials (Ionita, Pandele, & Iovu, 2013). Graphene nanosheets have been considered as better nanofiller for the preparation of the polymer composite materials. Graphene is a two dimensional sheet of sp^2 hybridized carbon atoms which has attracted tremendous attention (Wintterlin & Bocquet, 2009) because it is non-toxic and has exceptional physical properties (Geim & Novoselov, 2007).

Graphene/graphene oxide (GO)–polymer composites exhibit a significant increase of elastic modulus, tensile strength, thermal stability and electrical conductivity even at low loading of graphene filler (Ionita et al., 2013; Steurer, Wissert, Thomann, & Mulhaupt, 2009). The highest properties enhancement is achieved when the nanofiller is homogeneously dispersed in the polymer matrix and the interaction between the filler and the matrix is strong.

Chitosan (CS), a natural polymer extracted by the exoskeleton of crustaceans, is widely investigated for biomedical applications because of its good biocompatibility, biodegradability, bioadhesivity and antibacterial properties (Fang, Long, Zhao, Wang, & Chen, 2010; Goktepe, Celik, & Bozkurt, 2008). Chitosan based materials can be obtained in different forms like films, hydrogels, fibers and micro/nanoparticles. However, some major drawbacks such as low mechanical strength and processability restrict its use for scaffolds in tissue engineering (Carson et al., 2009).

Poly(vinyl alcohol) (PVA) is a non-toxic water soluble polymer with good physical and chemical properties (Dias, Mansur, Dannici, & Pereira, 2011; Wang, Wang, Xu, Zhang, & Shang, 2011). It could be blended with different synthetic and natural polymers due to its high hydrophilicity and processability (Han, Yan, Chen, & Li, 2011). The bioinert character of PVA, determined its broadly use in biomedical field such as drug delivery, hemodialysis, and implantable medical device.

In our previous works (Ionita & Iovu, 2011) we demonstrated that by combining a biopolymer such as CS with PVA some of the CS drawbacks mentioned above are overcome. However, the extent of properties improvement was not as high as expected. Our approach in the present paper is to take advantage of complementary

* Corresponding author. Tel.: +40 740465637.
E-mail address: mariana.ionita@polimi.it (M. Ionita).

0144-8617/$ – see front matter © 2013 Elsevier Ltd. All rights reserved.
http://dx.doi.org/10.1016/j.carbpol.2013.10.085

properties of the three materials, biocompatibility associated with CS, processability and versatility associated with PVA and exceptional physical properties of graphene/graphene oxide in order to obtain a composite material which merges the above-mentioned properties. Nonetheless, poor dispersability and strong aggregation of graphene layers within a polymer matrix challenge their use in the fabrication of the graphene–polymer composite materials. Both dispersability and interaction formation are mediated by the graphene modification. In the absence of a facile method for chemical modification the use the graphene oxide is an effective approach in this regard. The use of graphene oxide is expected to enable its readily dispersion in polymer matrices. Moreover, the hydroxyl functionalities available on graphene surface could be employed in formation of H-bonds with hydroxyl functionalities of the PVA and CS. Incorporation of GO within chitosan is an active approach for improving the physical and chemical properties of chitosan. Currently, to the best of our knowledge, there have been no reports on the integration of GO within CS–PVA blend. Since PVA presents a flexible backbone with numerous hydroxyl groups we believe that interfacial bonding with both hydroxyl groups of GO and CS could be facilitated. Interfacial bonding GO/CS is difficult to be realized due to the limited number of active sites which just occasionally are in feasible positions (steric hindrance).

In this paper, we report a simple and effective method for the fabrication of thin films based on incorporation of graphene oxide (GO) in CS–PVA blend. The composites were prepared using various concentration of graphene oxide. The as-synthesized thin films were characterized by Fourier Transform Infrared Spectroscopy (FT-IR), Thermogravimetrical Analysis (TGA), Raman Spectroscopy, X-Ray Diffraction analysis (XRD), Transmission Electron Microscopy (TEM) and Scanning Electron Microscopy (SEM). Furthermore, the mechanical properties and biocompatibility of CS–PVA/GO films were explored.

2. Experimental

2.1. Chemicals and reagents

Graphene oxide was purchased from National Institute for Research and Development in Microtechnologies (Romania) and prepared according to Hummers method (Hummers & Offeman, 1958). Acetic acid (≥99.7%), chitosan from crab shells and poly(vinyl alcohol) were supplied from Sigma Aldrich. All materials were used without future purification.

2.2. Preparation and characterization of PVA–chitosan/graphene oxide composite films

Chitosan was mixed with acetic acid solution (10% by weight in water) at ~50 °C in order to form 1 wt.% homogenous viscous solution. Separately, 1 wt.% PVA aqueous solution was obtained by dissolving PVA powder in distilled water at 120 °C in an autoclave. Blends were prepared by mixing the two polymer solutions (50:50, v/v ratio). The composite mixtures with different GO amount (0.5, 1, 2.5, 6 wt.%) were prepared by gradually adding the GO solution (1 mg/ml in water) to the CS–PVA solution and sonicating for 1 h at room temperature. The homogeneous CS–PVA/GO solutions were poured onto transparent Petri glass dish and left undisturbed at room temperature for 72 h in order to evaporate the solvent and form the film. After that the films were peeled off from the mold and thermal treated *in vacuum* according to the following procedure: 30 min at 50 °C, 30 min at 70 °C and over the night at 120 °C.

The structure of the nanocomposites was investigated by Fourier transform infrared (FT-IR) measurements, preformed on a SHIMADZU 8900 equipment. The FTIR spectra were recorded in 600–4000 cm^{-1} range with 4 cm^{-1} resolution. The samples were analyzed from ATR. Raman spectra were performed on a DXR Raman Microscope from Thermo Scientific using a 633 nm laser line and a number of 10 scans. The laser beam was focused with the 10× objective of the Raman microscope. The X-ray diffraction analysis (XRD) was done on a Panalytical X′Pert Pro MPD instrument with CuKα radiation. Thermogravimetrical analysis (TGA) curves were registered on a Q500 TA Instruments equipment, using nitrogen atmosphere from room temperature to 600 °C and a heating rate of 10 °C/min. The morphology of the films was investigated on a QUANTA INSPECT F scanning electron microscope (SEM) equipped with field emission gun (1.2 nm resolution) and with an energy dispersive X-ray spectrometer with a resolution of 133 eV to MnKα. The composite films structure was further characterized by transmission electron microscopy (TEM), the images being recorded on a TECNAI F30 G2 S-TWIN equipment provided with 300 kV emission gun.

Mechanical tests were done using a universal mechanical tester (Instron, Model 3382, USA) at a relative humidity of 45–50% and a speed of 2 mm/min. The size of the sample was 10 cm in length and 1 cm in width. A minimum of six to eight specimens was tested for each composite film and the average values are reported.

2.3. Biocompatibility of PVA–chitosan/graphene oxide composite films

Mouse osteoblastic cell line MC3T3-E1 (ECACC, code 99072810) was used as an *in vitro* cellular model for biocompatibility assessment. Bidimensional cell cultures were obtained by seeding an initial density of 2.5×10^4 cells/cm^2 on films surface. *In vitro* cell cultures were kept in standard conditions (37 °C, 5% CO_2 and 95% humidity), in adequate media formulation, minimum essential medium eagle (MEM) alpha culture medium, supplemented with 2 mM glutamine and 10% fetal bovine serum (FBS). All performed tests were compared with a bidimensional cell culture on plastic surface (2D control) and a bidimensional culture on CS–PVA film (control).

The percentage of viable cells and the cells rate proliferation on the surface of the CS–PVA/GO composite materials was determined using fluorescence microscopy and Live/Dead Kit (Invitrogen, Life Technologies, Foster City, CA, L3224). The method allows the simultaneous detection of both living and dead cells based on two dyes, calcein AM and ethidium bromide. Live/dead fluorescence microscopy assay was performed after 2, 4 and 7 days of culture by fluorescence microscopy using an Olympus IX71 inverted microscope and images were captured with Cell F Imaging Software (Olympus). 3-(4,5-dimethylthiazol-2-yl)-2,5-diphenyltetrazolium bromide (MTT) spectrophotometric test was used to quantitatively assess cell viability at 2, 4 and 7 days post seeding. The cells cultured on CS–PVA/GO films and their controls were incubated with 1 mg mL^{-1} of MTT for 4 h. The resulted formazan salts were dissolved in isopropanol and the absorbance was measured at 550 nm using ThermoScientific Appliskan plate reader.

The cytotoxic potential of the CS–PVA/GO materials on the osteoblasts was evaluated using *in vitro* toxicology assay kit lactate dehydrogenase based (LDH) (Sigma Aldrich Co., Steinheim, Germany, code TOX7-1KT). The culture media were harvested at 2, 4 and 7 days post seeding and they were mixed with the solutions provided in the kit. After 20 min of incubation, the reaction was stopped with 1 N hydrochloric acid (HCl) and the LDH concentration was determined by measuring the optic density of the resulting solution at 490 nm (Appliskan Thermo Scientific).

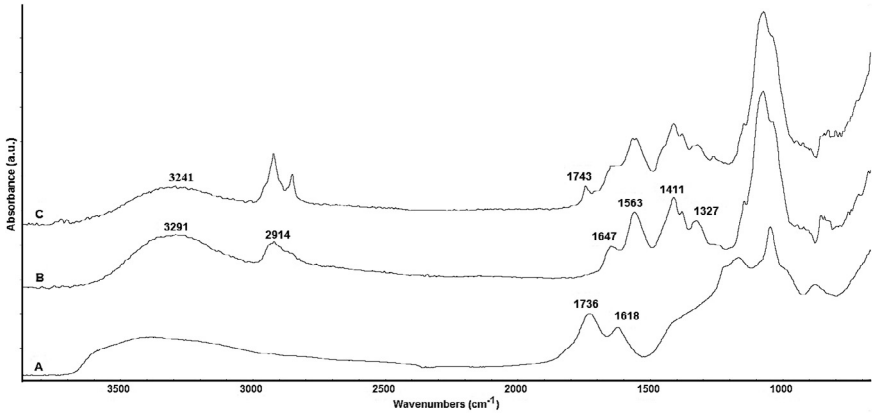

Fig. 1. FT-IR spectra of the (A) GO, (B) CS–PVA, and (C) CS–PVA/GO 2.5 wt.%.

3. Results and discussion

3.1. Structural and morphological characterization

The FT-IR experiments were performed to investigate the interaction between the CS–PVA and GO. The FT-IR spectra of CS–PVA, GO, and CS–PVA/GO (2.5 wt.%) biocomposite films are shown in Fig. 1. GO spectrum (Fig. 1A) displays two characteristics bands at 1736 and 1618 cm^{-1} assigned to C=O stretching vibration of the carboxylic group and C=C stretching mode of the sp^2 network (Zhang et al., 2011). CS–PVA blend exhibits FT-IR absorption bands around 3291 and 2914 cm^{-1}, concerned —OH stretching and —CH_2 asymmetric stretching from PVA. The peaks at 1647, 1563, and 1327 cm^{-1} are assigned to amide I and III of C=O stretching vibration, N—H bending of —NH_2 and —CH_2 wagging coupled with OH group from CS. The peak at 1411 cm^{-1} corresponds to oscillations of —OH and —CH groups (Jia et al., 2007). In comparison with CS–PVA blend spectrum, CS–PVA/GO composite spectrum (Fig. 1C) presents new peak at 1743 cm^{-1} assigned to carboxyl groups from GO surface which indicates the presence of GO within the PVA-CS blend. Furthermore, the peak at 3291 cm^{-1} (O—H stretching vibration) was shifted to lower values (3241 cm^{-1}) and becomes more broadened which can be attributed to the hydrogen-bonding interaction of GO with CS–PVA blend.

Fig. 2 shows the Raman spectra of pristine GO and CS–PVA/GO composite films. In the GO spectrum two peaks at ~1349 and ~1591 cm^{-1} assigned to D band and G band are observed. The D band indicates the disorder in the GO structure while G band corresponds to the ordered sp^2 bonded carbon (Fang et al., 2010). From Fig. 2B and C, it can be observed that CS–PVA/GO composites exhibit a similar spectrum with the pristine GO, with a slight shifting of D and G band to ~1340 and 1602 cm^{-1}, respectively. In addition, by increasing the GO content in the CS–PVA/GO composite material the Raman D to G intensity ratio decreases (Table 1).

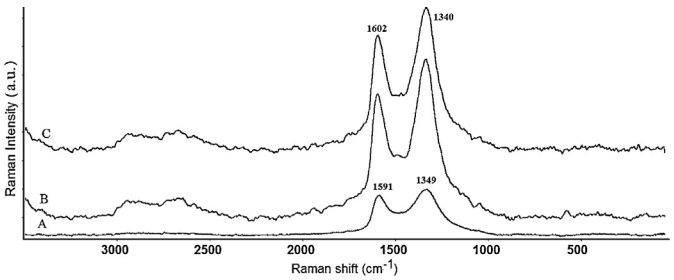

Fig. 2. Raman spectra of (A) GO, (B) CS–PVA/GO composite film with 1 wt.% GO content and (C) CS–PVA/GO composite film with 6 wt.% GO content.

Table 1
The I_D/I_G of GO and the CS–PVA/GO composite films.

Sample	GO content (wt.%)	I_G[a]	I_D[a]	I_D/I_G[a]
GO	0	29.30	32.10	1.09
CS–PVA/GO	1	135.54	205.40	1.51
CS–PVA/GO	2.5	130.27	171.74	1.32
CS–PVA/GO	6	116.10	152.39	1.31

[a] I_D intensity of D band, I_G intensity of G band, I_D/I_G intensity ratio of D band to G band.

The intensity ratio of D and G band (I_D/I_G) is used to measure the distance between the defects in the GO structure (Eigler, Dotzer, & Hirsch, 2012). Cancado et al. (2011) noted that the ratio of the D to G band intensities varied inversely with the crystallite size. The decrease of the D to G intensity ratio as the GO content increase in the composite material is attributed to an increase of the size of the CS–PVA crystallite and moreover, to an increase of crystallinity in the composite material as the GO amount increase.

The crystallinity of the CS–PVA/GO composites was further examined by XRD investigations. GO spectrum (Fig. 3A) exhibits

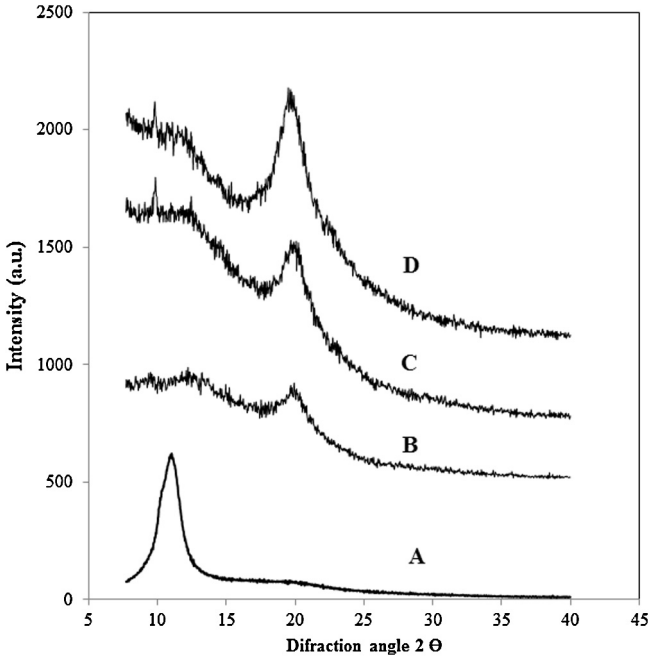

Fig. 3. XRD patterns of (A) GO; (B) CS–PVA; (C) CS–PVA/GO 2.5 wt.%; (D) CS–PVA/GO 6 wt.%.

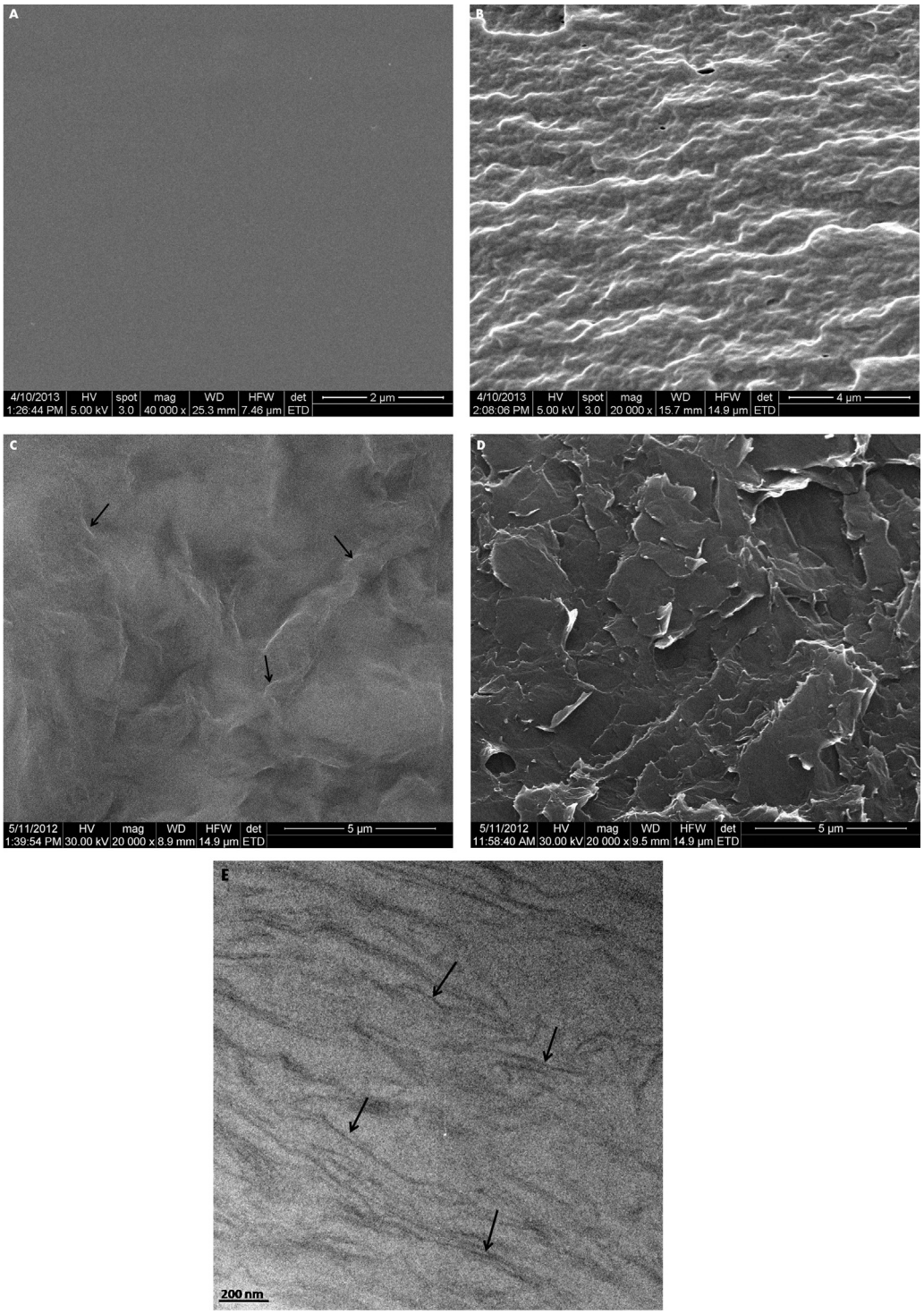

Fig. 4. (A) SEM image of the CS–PVA film surface, (B) CS–PVA film fracture surface, (C) CS–PVA/GO 2.5 wt.% film surface, (D) CS–PVA/GO 2.5 wt.% film fracture surface, and (E) representative high-resolution TEM micrograph of the CS–PVA/GO 2.5 wt.%.

a characteristic diffraction peak at $2\theta = 10.92^\circ$ corresponding to a d spacing of 8.06 Å according to Bragg equations (Li et al., 2012). The XRD pattern of CS–PVA blend shows two weak diffraction peaks located at $2\theta = 9.03^\circ$ and 11.9° assigned to CS indicating an almost amorphous structure for this compound. The peak appearing at $2\theta = 19.82^\circ$ belongs to PVA crystallites (Lu, Peng, Jiang, & Wang, 2006). In the CS–PVA/GO composite films spectra (Fig. 3C and D) it is observed that the incorporation of the GO obviously increase the intensity and sharpness of the characteristic peaks of CS ($2\theta = 9.45^\circ$ and $2\theta = 11.87^\circ$). Moreover, there is an increase in intensity of the peak centered at $2\theta = 19.82^\circ$ corresponding to PVA as the GO content increases in the polymer blend. The absence of the characteristic peak of GO is indicating that most GO sheets were dispersed within polymer matrix, or the peak is weak (just low content of GO aggregates are formed) and overlapped by the peak of CS at $2\theta = 9.45^\circ$. X-ray diffraction pattern clearly illustrates that the incorporation of GO affect the crystalline structure of CS–PVA. Similar behavior was found for other nanocomposites polymer/carbon

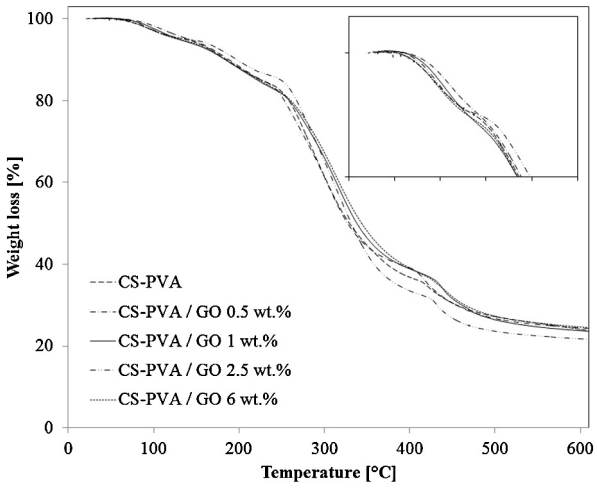

Fig. 5. The TGA curves of CS–PVA and CS–PVA/GO nanocomposites. Inset: Magnification of first stage of degradation.

nanofiller and is believed to be a result induced by the carbon nanofiller (Ionita et al., 2013; Yang, Tu, Li, Shang, & Tao, 2010). In this particular case, CS–PVA/GO composite films, the increase of the polymer blend crystallinity could be attributed to the intermolecular hydrogen bonding, confirmed by FT-IR, between CS–PVA blend and GO which could give a relatively ordered adjustment of the polymer chains along the GO nanosheets.

The morphology of the composite films was characterized by SEM and TEM techniques. Fig. 4C and D exhibits a typical SEM image of surface and the cross-section of the CS–PVA/GO composite films. Unlike the pure polymer (Fig. 4A and B), which structure is smooth, the morphology of the nanocomposite changes, becomes rough and exhibits little wrinkles assigned to the GO nanosheets presence.

The TEM investigation confirms the homogenous dispersion of GO sheets within polymer matrix with hardly any aggregations for lower GO contents (0.5 and 1 wt.%). Conversely, it seems that the GO content increase to 2.5 and 6 wt.% leads to isolated aggregation of the nanofiller (Fig. 4E). The orientation of the GO nanosheets seems to be almost parallel distributed to the biocomposite film surface. We have reported an analogous behavior for similar materials; the formation of lamellar structure for sodium alginate/GO composite material obtained by a similar preparation method (Ionita et al., 2013).

3.2. Thermal and mechanical characterization

The interest in CS–PVA reinforced composites stem from their potential applications in biomedical field such as bone repair; utilization which requires good thermal and mechanical properties coupled with excellent biological activity. The observed good dispersion of GO within CS–PVA matrix showed by SEM, TEM and XRD combined with hydrogen bond interaction between GO and CS–PVA polymer chains, evidenced by FT-IR spectrometry, is anticipated to produce an enhancement of mechanical and thermal properties of the materials. Moreover, the presence of the GO produced modification of materials surface (from smooth to rough) which can facilitate the cells attachment. On the other hand GO nanosheets from the film surface could act as anchors for cells.

The thermogravimetrical analyses were used to explain the CS–PVA blends thermal behavior with GO loading. The TGA curves of pure CS–PVA blend and the CS–PVA/GO composite films with various contents of GO were outlined in Fig. 5. As can be seen, both pure CS–PVA films and the composite present three decomposition steps. The first step between 70 and 150 °C is due to the moisture inside the film. The second degradation step starts at 150 °C and it ends at 390 °C and is assigned to the decomposition of the polymer structure. The final stage is attributed to the further decomposition of the residue (Jiang, Shen, Wu, & Shen, 2010). When GO is loaded into the polymer matrix the degradation stages were shifted toward higher values of temperature. The $Td_{3\%}$ (temperature at which the mass loss is 3%) values obtained for the pure CS–PVA and the composites are summarized in Table 2. The $Td_{3\%}$ increased by about 7–12 °C in the case of the composite with lowest (0.5 and 1 wt.%) amount of GO due to the good dispersion of the filler into CS–PVA matrix and the presence of hydrogen interaction between CS–PVA chains and GO which suppress the polymer chain mobility. However, as the GO loading further increases, the tendency for $Td_{3\%}$ is to decrease and even reach slightly lower value than for the net CS–PVA probably due to the aggregation of GO within the polymer blend.

Table 2
$Td_{3\%}$ and tensile modulus of CS–PVA blend and CS–PVA/GO nanocomposites.

Sample	GO content (wt.%)	$Td_{3\%}$ (°C)	Tensile modulus (GPa)
CS–PVA	0	103	1.83 ± 0.21
CS–PVA/GO	0.5	115	1.96 ± 0.26
CS–PVA/GO	1	110	2.18 ± 0.25
CS–PVA/GO	2.5	104	4.64 ± 0.51
CS–PVA/GO	6	101	5.78 ± 0.85

The mechanical behavior of the CS–PVA blend and CS–PVA/GO composite materials with different content of GO was further characterized by tensile tests. The representative tensile stress *versus* strain curves are reported in Fig. 6 and the average (measured for 6–8 samples) tensile modulus are listed in Table 2. An improvement of the mechanical performance of the nanocomposites compared to pure CS–PVA matrices was observed. By adding a small amount of GO within the CS–PVA matrix just a marginal effect was observed, the tensile modulus increased from 1.83 to 1.96 GPa. By further increasing the GO content in polymer matrix a significant increase of the tensile modulus was observed, *e.g.* loading 6 wt.% GO within CS–PVA matrix generated an increase by about 200% of the tensile modulus. This trend is however normal and ascribed to the interaction between GO and CS–PVA matrix and the change in the crystallinity, which are both important factors for the enhancement of tensile properties of a polymer. This findings could be also correlated with the largely good dispersion of GO within the polymer matrix which leads to a more uniform stress distribution and minimizes the presence of the stress concentration centers (Yang et al., 2010). The incorporation of GO affects the crystallinity of CS–PVA as indicated by XRD and Raman spectroscopy pattern. The addition of 2.5 and 6 wt.% of GO produced and important change of the

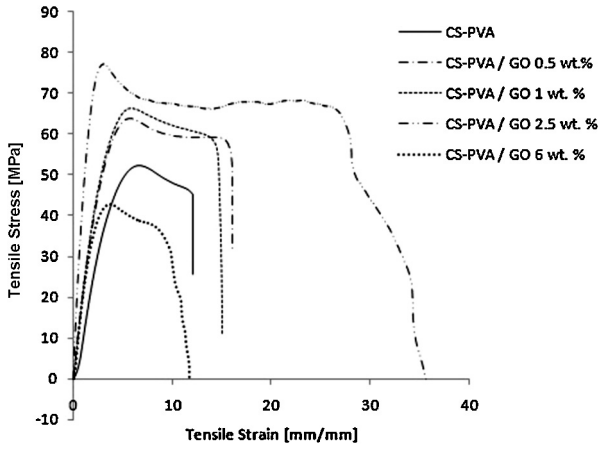

Fig. 6. Tensile strain *versus* tensile stress of CS–PVA and CS–PVA/GO films.

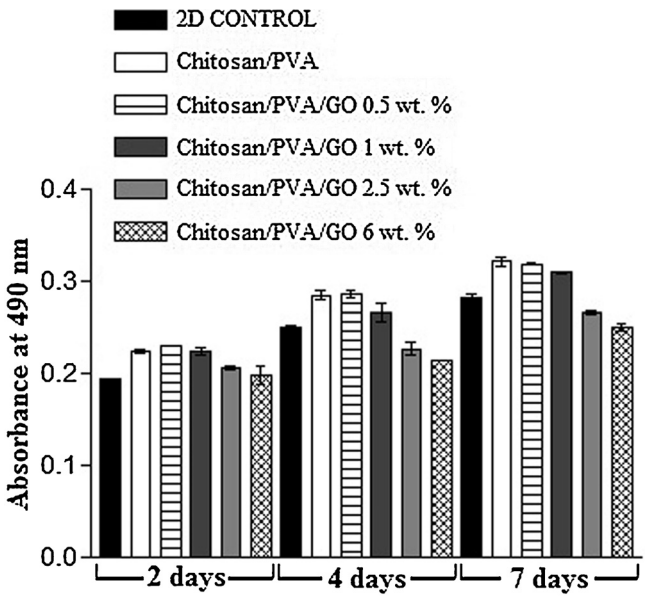

Fig. 7. The cytotoxic potential of the CS–PVA/GO films in contact with osteoblasts at 2, 4 and 7 days of culture, as revealed by LDH assay.

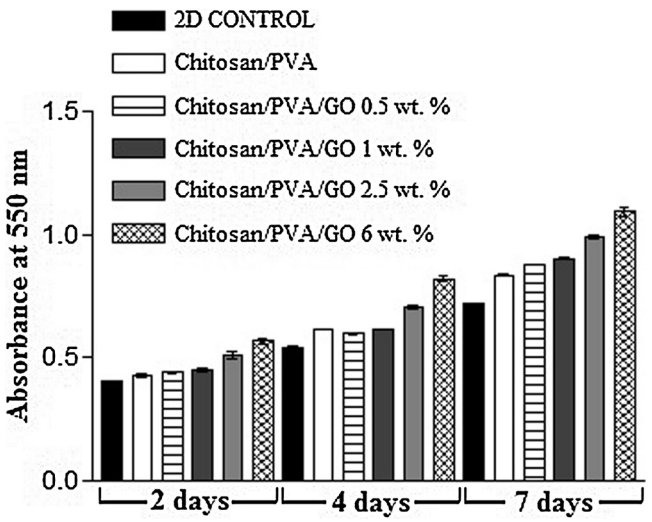

Fig. 8. The quantification of cell proliferation rate on CS–PVA/GO films as revealed by MTT test at 2, 4 and 7 days of culture.

crystalline structure of the CS–PVA and significant increased the tensile modulus of composites. The incorporation of less than 1 wt.% GO only slight affect the crystalline structure of CS and produced insignificant increase of the tensile modulus of the composites. Similar findings have been revealed for carbon nanotubes (Zhang et al., 2003) and GO based composites (Yang et al., 2010), whereas the largest improvement of tensile modulus was observed for the composites in which a great increase of crystallinity of the polymer was observed.

3.3. Biocompatibility assessment

All materials were tested for cytotoxicity in contact with murine osteoblasts during one week of culture. Although all samples displayed low cytotoxicity at 2, 4 and 7 days, the CS–PVA/GO composites with 2.5 and 6 wt.% GO content showed a significantly lower cytotoxic potential than CS–PVA/GO composites with 0.5 and 1 wt%. The samples with 0.5 and 1 wt.% GO registered the same levels of LDH released in the culture medium as the control and CS–PVA blend (Fig. 7). Thus, the addition of 0.5 and 1 wt.% graphene oxide in the composition of CS–PVA film apparently has no significant impact on the material's cytotoxicity. Conversely, the samples with 2.5 and 6 wt.% GO revealed a similar cytotoxic potential at 2 days of culture as compared to the control. However, at 4 and 7 days of culture, LDH levels measured for composite films with 2.5 and 6 wt.% GO were found to be lower than the levels registered for control. Consequently, CS–PVA/GO 6 wt.% displayed the lowest cytotoxic potential among the studied compositions, which may suggest that the addition of graphene oxide in the structure of chitosan films enhances material biocompatibility in contact with cells and ensures a favorable microenvironment for cell viability and proliferation. LDH levels registered on the pure CS–PVA control were significantly higher ($p < 0.01$) than the LDH released in 2D system during one week of culture in standard conditions. This variation could be attributed to the significant difference between the two culture systems in terms of initial cell seeding density on each system as well as cell interactions with the substrates and with external factors such as diffusion of oxygen, nutrients, *etc.* Samples containing 0.5 and 1 wt.% GO revealed no significant differences regarding cytotoxicity potential when compared to the pure CS–PVA control or between them for all (2, 4 and 7 days) studied period, suggesting that the addition of low GO amount did not influence cell behavior in contact with the materials. However, when adding 2.5 wt.% GO to the CS–PVA matrix, statistically significant lower cytotoxic potential was observed after 2 days of culture ($p < 0.01$) when compared to the CS–PVA control or to the composites with lower GO content. The difference between samples increased at 4 and 7 days of culture ($p < 0.001$). According to our study, CS–PVA/GO 6 wt.% appeared to be the sample with the lowest cytotoxic potential among the studied samples, since after 2, 4 and 7 days of culture it released the lowest amount of LDH in the culture medium. Statistically, the differences registered when comparing them to CS–PVA control or to the low GO content composites during all 7 days of culture were highly significant ($p < 0.001$), but with a lower significance ($p < 0.05$) when related to CS–PVA/GO 2.5 wt.%.

Quantitative MTT test revealed cell viability and proliferation on all studied samples (Fig. 8). An increasing cell proliferation potential was generally observed during 7 days of culture in standard conditions. Murine osteoblasts were able to proliferate on the surface of the tested materials, generating cell monolayers on all composites. However, the proliferation potential was proved to be higher for cells cultivated on the surface of the CS–PVA and CS–PVA/GO films, as compared to the classical bidimensional (2D) culture. At 2 days post-seeding, cell viability for CS–PVA/GO 0.5 and 1 wt.% composite films and the controls was similar. Significant differences were observed for CS–PVA/GO composite film with 6 wt.% GO content, for which the highest cell viability at 2 days of culture was registered. Furthermore, the quantification performed after 4 and 7 days of culture revealed the same cell viability and proliferation pattern, with a higher proliferation rate for osteoblasts cultivated on CS–PVA/GO composite films with 2.5 and 6 wt.% GO content, as compared to the materials with lower GO content. In terms of cell viability and proliferation, the best sample was found to be CS–PVA/GO 6 wt.%, suggesting that a higher percent of GO added leads to better biocompatibility and cell bioactivity than in the absence of GO.

Statistical analysis of viability/proliferation data revealed important differences between the composites with low GO content (0.5 and 1 wt.%) and the composites with high GO (2.5 and 6 wt.%) content. Neat CS–PVA control and composites with 0.5 and 1 wt.% GO registered a similar increasing proliferation profile during one week of culture with a significant rate of increase ($p < 0.001$) in time. Conversely, when comparing CS–PVA/GO 2.5 wt.% with the low GO content composites, statistically significant difference was

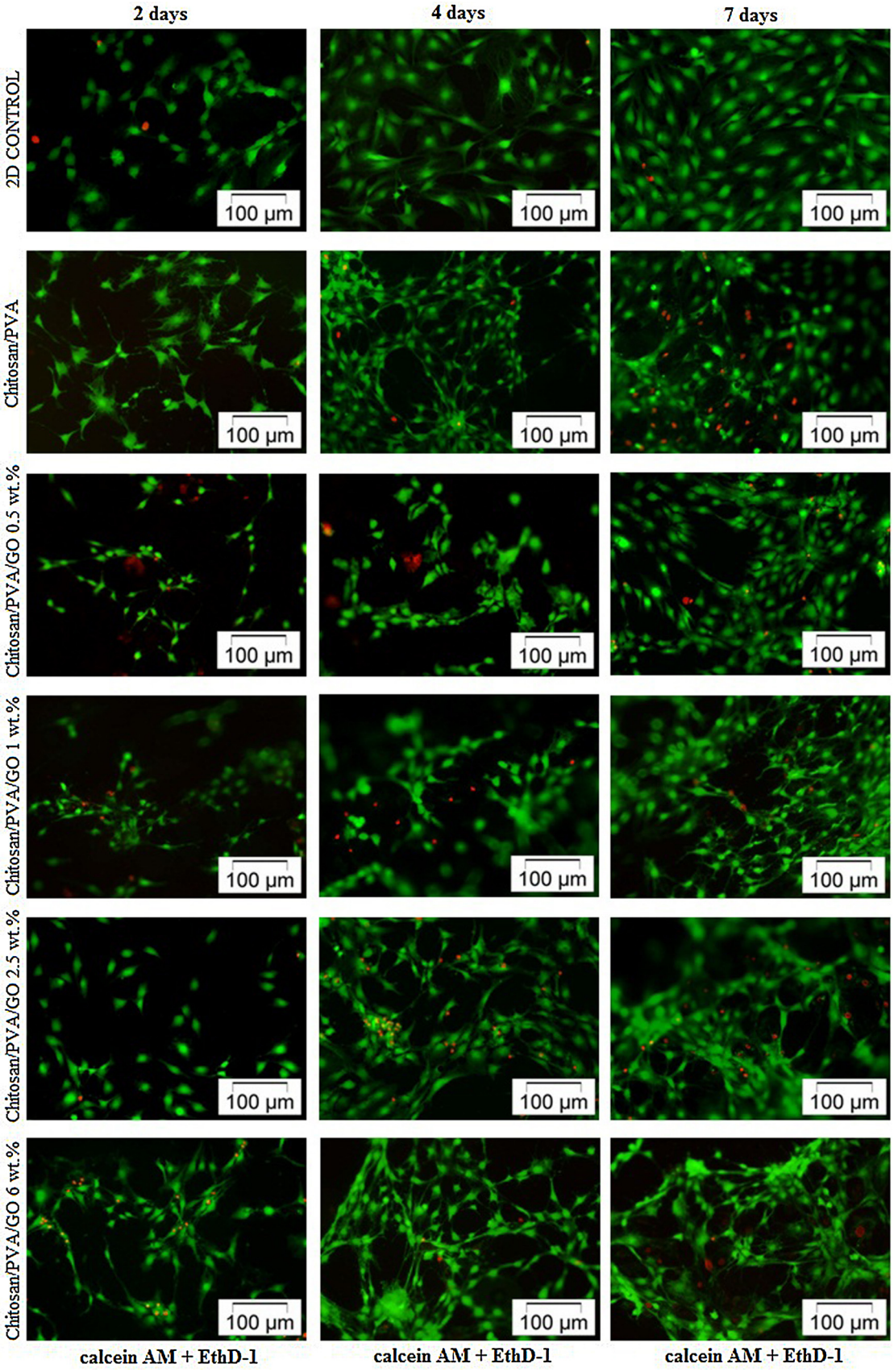

Fig. 9. Fluorescence microscopy evaluation of living (green-labeled) and dead (red-labeled) murine osteoblasts at 2, 4 and 7 days post-seeding on CS–PVA and CS–PVA/GO films. (For interpretation of the references to color in this figure legend, the reader is referred to the web version of the article.)

obtained at 2 ($p < 0.01$), 4 and 7 days of culture ($p < 0.001$). Increasing proliferation profile was also found for CS–PVA/GO 6 wt.% sample, which proved to have the highest cell viability and proliferation rate among the studied samples. After 2 days of culture in standard conditions, this sample revealed higher viability ($p < 0.001$) as compared to the neat CS–PVA control and to the samples with low GO content (0.5 and 1 wt.%) or to the composite with 2.5 wt.% GO ($p < 0.05$). The difference increased over time, at 4 and 7 days after cells culture CS–PVA/GO 6 wt.% revealed highest proliferation rates ($p < 0.001$), as compared to all other samples.

Cell behavior (viability, morphology, distribution) was qualitatively assessed after 2, 4 and 7 days of culture by fluorescence microscopy, based on the simultaneous staining of live and dead cells (Fig. 9). The results obtained by Live/Dead assay confirmed the quantitative determinations performed during MTT and LDH tests, concluding that CS–PVA/GO composite films with higher percentage of GO in their composition display higher biocompatibility that the ones with low GO content. Briefly, it was observed that cell behavior varies depending on the GO content. For example, cells displayed a particular morphology and distribution in lines on the surface of CS–PVA/GO 6 wt.%, as compared to the other samples and to the controls.

In terms of cell proliferation, it was observed a constant increasing cell number on all samples, suggesting a significant proliferation potential which cells displayed in contact with the tested materials. However, a lower cell number was found on the samples with 0.5 and 1 wt.% GO content at 2, 4 and 7 days, as compared to those with 2.5 and 6 wt.% GO content. This finding was correlated with the higher percent of dead (red-labeled) cells which was observed on the low-GO-containing materials, as compared to the rest of tested materials. Additionally, different cell morphology was revealed on the GO-containing materials than on the controls. Cell grouping tendency was revealed for the materials with higher GO content (2.5 and 6 wt.%), as observed in Fig. 9.

4. Conclusions

Mechanically strong with excellent biocompatibility CS–PVA/GO composite films have been successfully fabricated by solution blending method. It was observed by SEM, TEM and X-ray diffraction that graphene oxide is largely dispersed on molecular scale in the CS–PVA matrix. FTIR investigation indicated the occurrence of some interaction between graphene oxide nanosheets and CS–PVA blend. The composite film containing 6 wt.% GO showed highest tensile modulus of 5.78 GPa, which is about twice higher than that of neat matrix (CS–PVA). The composite films present a higher thermal stability when lower (0.5 and 1 wt.%) amount of GO was incorporate within CS–PVA matrix.

A higher content of GO within the composite film led to a significant increase of the cell proliferation rate. The CS–PVA/GO films with high mechanical strength, good thermal stability and excellent biological activity are competitive candidates for various biological applications, such as bone repair and tissue engineering.

Acknowledgments

This work was supported by a grant of the Romanian National Authority for Scientific Research, UEFISCDI, project number PN-II-PT-PCCA-140/2012.

References

Bianco, A., Kostarelos, K., & Prato, M. (2005). Applications of carbon nanotubes in drug delivery. *Current Opinion in Chemical Biology*, *9*(6), 674–679.

Cancado, L. G., Jorio, A., Ferreira, E. H. M., Stavale, F., Achete, C. A., Capaz, R. B., et al. (2011). Quantifying defects in graphene via Raman spectroscopy at different excitation energies. *Nano Letters*, *11*(8), 3190–3196.

Carson, L., Kelly-Brown, C., Stewart, M., Oki, A., Regisford, G., Luo, Z., et al. (2009). Synthesis and characterization of chitosan–carbon nanotube composites. *Materials Letters*, *63*(6–7), 617–620.

Depan, D., Shah, J. S., & Misra, R. D. K. (2011). Structure–process–property relationship of the polar graphene oxide-mediated cellular response and stimulated growth of osteoblasts on hybrid chitosan network structure nanocomposite scaffolds. *Acta Biomaterialia*, *7*(9), 3432–3445.

Dias, L., Mansur, L. S., Donnici, H. S., & Pereira, C. L. (2011). Synthesis and characterization of chitosan–polyvinyl alcohol-bioactive glass hybrid membranes. *Biomatter*, *1*(1), 114–119.

Eigler, S., Dotzer, C., & Hirsch, A. (2012). Visualization of defect densities in reduced graphene oxide. *Carbon*, *50*(10), 3666–3673.

Fang, M., Long, J., Zhao, W., Wang, L., & Chen, G. (2010). pH-responsible chitosan-mediated graphene dispersion. *Langmuir*, *26*(22), 16771–16774.

Geim, A. K., & Novoselov, K. S. (2007). The rise of graphene. *Nature Materials*, *6*, 183–191.

Goktepe, F., Celik, S. U., & Bozkurt, A. (2008). Preparation and the proton conductivity of chitosan/poly(vinyl phosphonic acid) complex polymer electrolytes. *Journal of Non-Crystalline Solids*, *354*(30), 3637–3642.

Han, D., Yan, L., Chen, W., & Li, W. (2011). Preparation of chitosan/graphene oxide composite film with enhanced mechanical strength in the wet state. *Carbohydrate Polymers*, *83*(2), 653–658.

Hummers, W. S., & Offeman, R. E. (1958). Preparation of graphitic oxide. *Journal of American Chemical Society*, *80*, 1339.

Ionita, M., & Iovu, H. (2011). Mechanical properties, urea diffusion, and cell cultural response of poly(vinyl alcohol)–Chitosan bioartificial membranes via molecular modelling and experimental investigation. *Composite Part B: Engineering*, *43*(5), 2464–2470.

Ionita, M., Pandele, M. A., & Iovu, H. (2013). Sodium alginate/graphene oxide composite films with enhanced thermal and mechanical properties. *Carbohydrate Polymers*, *94*(1), 339–344.

Jia, Y. T., Gong, J., Gu, X. H., Kim, H. Y., Dong, J., & Shen, X. Y. (2007). Fabrication and characterization of poly (vinyl alcohol)/chitosan blend nanofibers produced by electrospinning method. *Carbohydrate Polymers*, *67*(3), 403–409.

Jiang, L., Shen, X. P., Wu, J. L., & Shen, X. C. (2010). Preparation and characterization of graphene/poly(vinyl alcohol) nanocomposites. *Journal of Applied Polymer Science*, *118*(1), 275–279.

Li, X., Fan, Y., & Watari, F. (2010). Current investigations into carbon nanotubes for biomedical application. *Biomedical Materials*, *5*(2). Article ID 022001.

Li, L., Li, C., Qiong, J., Pengfei, X., Xiaoting, L., & Qiuping, Z. (2012). Preparation and characterization of chitosan/graphene oxide composites for the adsorption of Au(III) and Pd(II). *Talanta*, *93*, 350–357.

Lu, L., Peng, F., Jiang, Z., & Wang, J. (2006). Poly(vinyl alcohol)/chitosan blend membranes for pervaporation of benzene/cyclohexane mixtures. *Journal of Applied Polymer Science*, *101*(1), 167–173.

Steurer, P., Wissert, R., Thomann, R., & Mulhaupt, R. (2009). Functionalized graphenes and thermoplastic nanocomposites based upon expanded graphite oxide. *Macromolecular Rapid Communication*, *30*(4–5), 316–327.

Wang, J., Wang, X., Xu, C., Zhang, M., & Shang, X. (2011). Preparation of graphene/poly(vinyl alcohol) nanocomposites with enhanced mechanical properties and water resistance. *Polymer International*, *60*(5), 816–822.

Wintterlin, J., & Bocquet, M. L. (2009). Graphene on metal surfaces. *Surface Science*, *603*(10–12), 1841–1852.

Xiaodong, C., Hua, D., Chang, M. L., & Lucian, A. L. (2010). The enhanced mechanical properties of covalently bound chitosan-multiwalled carbon nanotube nanocomposite. *Journal of Applied Polymer Science*, *113*, 466–472.

Yang, X., Tu, Y., Li, L., Shang, S., & Tao, X.-M. (2010). Well-dispersed chitosan/graphene oxide nanocomposites. *ACS Applied Materials & Interfaces*, *2*(6), 1707–1713.

Zhang, X. F., Liu, T., Sreekumar, T. V., Kumar, S., Moore, V. C., Huage, R. H., et al. (2003). Poly(vinyl alcohol)/SWNT composite film. *Nano Letters*, *3*(9), 1285–1288.

Zhang, W., Zhou, C., Zhou, W., Lei, A., Zhang, Q., Wan, Q., et al. (2011). Fast and considerable adsorption of methylene blue dye onto graphene oxide. *Bulletin of Environmental Contamination and Toxicology*, *87*, 86–90.